Bioelectromagnetics. Author manuscript; available in PMC 2012 Sep 1.

Published in final edited form as:

Bioelectromagnetics. 2011 Sep; 32(6): 423–433.

Published online 2011 Feb 22. doi: 10.1002/bem.20658

PMCID: PMC3118398

NIHMSID: NIHMS274632

ENHANCED ABSORPTION OF MILLIMETER WAVE ENERGY IN MURINE SUBCUTANEOUS BLOOD VESSELS

Stanislav I. Alekseev and Marvin C. Ziskin

Author information ► Copyright and License information ►

The publisher's final edited version of this article is available at Bioelectromagnetics

Go to:

Abstract

The aim of the present study was to determine millimeter wave (MMW) absorption by blood vessels traversing the subcutaneous fat layer of murine skin. Most calculations were performed using the finite-difference time-domain (FDTD) technique. We used two types of models: (1) a rectangular block of multilayer tissue with blood vessels traversing the fat layer and (2) cylindrical models with circular and elliptical cross sections simulating the real geometry of murine limbs. We found that the specific absorption rate (SAR) in blood vessels normally traversing the fat layer achieved its maximal value at the parallel orientation of the E-field to the vessel axis. At 42 GHz exposure, the maximal SAR in small blood vessels could be more than 30 times greater than that in the skin. The SAR increased with decreasing the blood vessel diameter and increasing the fat thickness. The SAR decreased with increasing the exposure frequency. When the cylindrical or elliptical models of murine limbs were exposed to plane MMW, the greatest absorption of MMW energy occurred in blood vessels located on the lateral areas of the limb model. At these areas the maximal SAR values were comparable with or were greater than the maximal SAR on the front surface of the skin. Enhanced absorption of MMW energy by blood vessels traversing the fat layer may play a primary role in initiating MMW effects on blood cells and vasodilatation of cutaneous blood vessels.

Keywords: murine skin, FDTD technique, specific absorption rate

Go to:

INTRODUCTION

Millimeter waves (MMW) have been used for the therapeutic treatment of different medical conditions including cardiovascular diseases, wound healing, pain relief, etc. [Rojavin and

Ziskin, 1998]. Significant results were achieved with the application of three “therapeutic” frequencies: 42.25, 53.57 and 61.22 GHz at the incident power densities (IPD) of 10–30 mW/cm^2. This has stimulated great interest in better understanding the biological mechanisms of MMW action and accurate dosimetry of MMW exposures. In recent publications we have described MMW dosimetry for human and murine skin [Alekseev et al., 2008a, b]. Since most experiments with MMW were performed on mice, the determination of the power density distribution in murine skin was important in order to make adequate extrapolation of the MMW effects found in mice to humans. Due to the small size of murine skin, MMW penetrate deep enough into tissue to reach the muscle layer. Up to 40% of MMW energy entering the skin is absorbed by muscle. Hence, the blood vessels located in the dermis and traversing the fat layer are subjected to MMW exposure with relatively high intensity. Some papers showed that MMW could affect blood cells causing significant biological effects [Gapeev et al., 1996; Roshchupkin et al., 1996]. Therefore, the accurate determination of MMW absorption by cutaneous blood vessels is important in understanding the primary mechanisms of the biological action of MMW.

The skin structures such as blood vessels and appendages (hair and sweat ducts) with electrical properties different from the average electrical properties of skin tissues cause selective absorption of MMW energy and local distortion of the MMW field in their vicinity [Alekseev and Ziskin, 2001, 2009a]. In our models the skin was irradiated with a plane wave normally incident on the skin surface. We found that in blood vessels located in the human and murine dermis and oriented parallel to the E-field, the specific absorption rate (SAR) could exceed the average SAR in the surrounding dermis by ~40% [Alekseev and Ziskin, 2009a].

Some papers showed that small holes in thin hydrophobic films with low permittivity (Teflon, acryl glass) used for the formation of bilayer lipid membranes could significantly absorb microwave energy [Eibert et al., 1999; Alekseev et al., 2009b, 2010]. As the hydrophobic film was placed in an electrolyte, the hole was also filled with the same bulk electrolyte. The enhanced absorption of microwave energy occurred at the orientation of the hydrophobic film perpendicular to the E-field, with the cylindrical axis of the hole being parallel to the E-field. Similar conditions for the enhanced absorption of MMW energy by blood vessels in murine skin may occur when the blood vessels traverse the fat layer. The fat layer, having lower permittivity than the surrounding dermis and muscle, may simulate a low permittivity hydrophobic film, while a blood vessel traversing the fat layer may simulate the membrane-forming hole.

The blood vessels feeding the epidermis and dermis enter and exit the dermis through the fat layer. At the boundary between the dermis and hypodermis they form a network located parallel to the boundary surface [Bloom and Fawcett, 1968]. From one side of this network small vessels enter the hypodermis and nourish fat cells. From another side of the network vessels enter the dermis. The sizes of blood vessels of murine skin do not differ significantly from those of human skin [Zweifach and Kossman, 1937; Algire, 1954; Braverman, 1989]. The internal diameters of the capillaries in mice are in the range of 3–10 μm. The diameters of the deepest dermal vessels are generally 40 to 50 μm.

When flat areas of skin are irradiated with plane MMW at normal incidence the E- and H-field vectors are directed parallel to the skin surface, and hence, perpendicular to the blood vessels traversing the fat layer. However, during whole-body exposure in the far field

[Jauchem et al., 1999, 2004; Gapeyev et al., 2006, 2008] the orientation of the E-field with respect to the skin surface changes with the curvatures of the body parts. For example, the orientation of the E-field with the skin surface of limbs, fingers, and tail may vary from being perpendicular to being nearly parallel to the blood vessels traversing the fat layer. In some biological experiments, mice were exposed at the nose and limb areas in the near field of a horn antenna [Radzievsky et al., 2000, 2008]. In this case, the E-field around the nose and limbs may take any direction relative to the skin surface including the perpendicular direction. Therefore, it is important to evaluate the MMW energy absorption by blood vessels traversing the fat layer at different orientations of the E-field.

The aim of the present study was to determine the SAR and E-field distributions in blood vessels traversing the subcutaneous fat layer of murine skin exposed to a plane MMW.

MATERIALS AND METHODS

To calculate the E-field and SAR in blood vessels traversing the fat layer we used two types of models: a rectangular block of skin tissue (Model I) and a cylindrical model with circular or elliptical cross sections simulating a murine limb (Model II). Model I was purely theoretical. This model did not represent the whole of or a separate organ of animals; it reproduced just a small part of the body (limb, finger, etc.) being exposed to MMW. The orientations of the field vectors relative to the blood vessels in the fat layer used in the block model could occur in the limbs and other organs of animals as shown in simulations of MMW exposure of limbs. Because of its simple geometry, Model 1 is very useful in understanding the physics of MMW interactions with blood vessels. It allows us to evaluate the maximal SAR and E-field values achievable with the given geometries of skin tissues and blood vessels, especially when the diameter of blood vessels is extremely small (capillaries). Model II simulated separate organs (limbs) of animals.

Most calculations of the E-field and SAR distributions were performed using the 3D finite-difference time-domain (FDTD) technique [Kunz and Luebbers, 1993]. For estimation of the maximal SAR in the narrow blood vessels (capillaries), we used a quasistatic approximation [Olver, 1992].

A. Models used for FDTD calculations

In Model I, we used a rectangular block of murine tissue containing the epidermis plus dermis (skin), fat and muscle layers (Fig. 1). In most calculations the thicknesses of the epidermis plus dermis and fat layers were set equal to 0.25 and 0.2 mm, respectively. These values were within the range found for murine skin [Dang et al., 2005; Grover et al., 2007; Alekseev et al., 2008b]. To determine the dependence of the SAR on the length of a blood vessel equal to the thickness of a fat layer, the latter was varied in the range of 0.05–0.5 mm. All tissue layers were located parallel to the skin surface along the direction of a plane wave as shown in Figure 1. A blood vessel oriented parallel to the E-field was placed traversing the fat layer, and located 0.4–0.8 mm from the side of the block closest to the MMW source. This location corresponded with the penetration depth of the 30–80 GHz MMW used in our calculations. A blood vessel was modeled by circular cylinders of different diameters (0.01–0.4 mm) and lengths (0.05–0.5 mm). Because the arteries feeding the skin are often paired with veins [Bloom and Fawcett, 1968], we examined the influence of the distance between two blood vessels on the SAR inside the blood vessels.

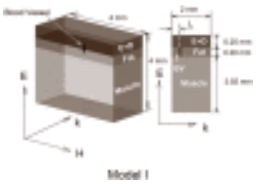

Figure 1

Model of a blood vessel traversing a fat layer of murine skin used in FDTD calculations of the E-field and SAR distributions. A block of murine skin consists of the epidermis plus dermis (E+D), fat, and muscle layers. The blood vessel (BV) is located **...**

The block was exposed to plane MMW normally incident on the front surface of the block with the E- and H-field components oriented parallel to the blood vessel and the fat layer plane, respectively. When studying the dependence of the SAR on the angle between the E-field and cylindrical axis of a blood vessel, the k-vector and E-field were rotated around the H-axis in the range of 0–90°. Though the SAR or E-field distortions were localized in the blood vessel region in the surrounding tissues, they still occupied some regions in tissues. Therefore, the size of the block was chosen to include all the distortions of the SAR in order to obtain a complete depiction of SAR changes. In most calculations it was 4×4 mm in the E-H plane. The thickness of the block was 2 mm, which was enough to eliminate the influence of the standing wave due to reflection from the rear surface of the block.

We used a perfect matching layer (PML) as the outer boundary condition for FDTD. In the E- and H-field directions the surrounding absorbing medium was in direct contact with the object, i.e., there was no free space between the object and PML boundaries. In the k-direction, in order to propagate the plane wave, we inserted free space between the object and the MMW source. Thus, the discrete tissue block in lateral directions was not surrounded by free space and can be considered as a part of an infinite object without resonance absorption characteristics.

In typical biological experiments, different animal sites (nasal area, limb and paw) were exposed to a plane wave. To simulate MMW exposure of murine limbs we developed cylindrical and elliptical models. Model II, consisting of cylindrical (elliptical) layers of skin, fat, and muscle, is shown in Figure 2. The external diameter of the cylinder was 3, 4 or 5 mm; the length was 2 mm. To simulate infinity along the cylinder axis we applied periodic boundary conditions [Maloney and Kesler, 1998]. The thicknesses of different layers were equal to those used in the previous model (Fig. 1). The model also included a cylindrical bone of different diameters (0, 1.5, 2.0 and 2.5 mm). We inserted the blood vessels traversing the fat layer in the radial direction, spaced at 15 angular degrees apart (α=0°, ±15°…±180°). This was done to find the areas of the limb where the maximal absorption of MMW by blood vessels would occur. The cylindrical (elliptical) model was exposed to a 42 GHz plane wave directed perpendicular to the cylinder axis. The H-field component was directed along the cylindrical axis. The ratio of the minor axis to the major axis of the elliptical model was 0.75. The major axis of the external ellipse was 4 mm.

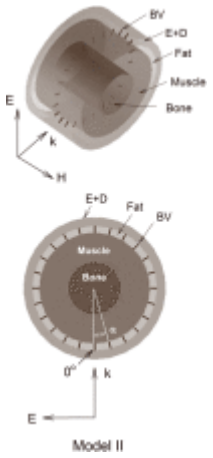

Figure 2

Cylindrical model of the murine limb used in FDTD calculations of the E-field and SAR distributions. The model consists of the epidermis plus dermis (E+D), fat, and muscle layers as well as cylindrical bone. The blood vessels (BV) traverse the fat layer **...**

Numerical calculations were performed for a plane wave in a scattered field using a commercially available FDTD program (xFDTD version 6.6, Remcom, St. Louis, MO, USA). The mesh cell size for the proposed geometries of blood vessels was 0.0012–0.025 mm, which is far less than one-tenth of a wavelength in associated cells, and automatically satisfies the commonly applied constraints on the cell size. The time step for the mesh cell size of 0.012 mm typically used in our calculations was 24 fs, which satisfied the restriction on the time step to ensure stability. The maximal frequency that could be used for good results was 2.4 THz. The frequencies used in calculations (30–80 GHz) were significantly lower than the maximal frequency. For all calculations the convergence threshold was set at −40 dB. To reach this accuracy, the number of iterations was within 8000–9000 for 40–50 GHz. At lower frequencies, the number of iterations increased by about 30%, at higher frequencies it decreased by about 10%.

We described some checks of validity of modeling MMW absorption by dermal blood vessels in our previous paper [Alekseev and Ziskin, 2009a]. We compared the SAR distribution in the skin and sphere with the permittivity equal to that of blood, calculated using the same FDTD program at different cell sizes with that obtained analytically. We found that the agreement between the analytical and numerical solutions was improved by reducing the cell size. A good match of the SAR profile calculated numerically to the analytical one (mean square error about 1%) was achieved at the cell size of 0.012 mm.

The SAR was determined by the following well-known expression:

$$SAR=\sigma \cdot E22\rho$$

(1)

where σ is the conductivity of tissue, E is the electric field amplitude, and ρ is the tissue density. To compare results calculated under different conditions, the SAR values in a blood vessel were normalized (nSAR) to those in the skin layer that were located sufficiently far from the blood vessel to have an undistorted uniform SAR (Fig. 3(a)). The IPD in all calculations was 10 mW/cm^2.

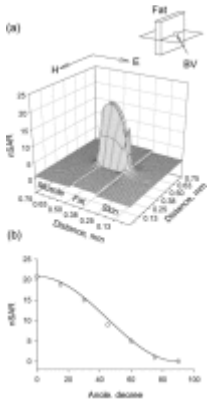

Figure 3

Normalized SAR distributions in a blood vessel and surrounding tissue. (a) 3D graph of the SAR distribution on a horizontal E-H plane cross-sectioning the fat layer at the center of the blood vessel (BV) as shown above. The E-field is directed along the **...**

The values of the electrical properties of murine tissues used in the calculations at each frequency are provided in Table 1. The values of ε′ and σ of the murine epidermis and dermis were selected in accordance with Alekseev et al. [2008b]. The values chosen for ε′ and σ of the blood, fat, muscle, and bone were given by Gabriel et al. [1996]. For bone, ε′ and σ at 42 GHz were 6.1 and 11.0 S/m, respectively. The mass density ρ for the skin, muscle, and blood was set equal to 1000 kg/m^3; for the fat, it was 850 kg/m^3 [Duck, 1990].

Table 1

Electrical properties of tissues at different frequencies.

f	Skin			Fat			Muscle		Blood	
	ε′	σ	|ε|	ε′	σ	|ε|	ε′	σ	ε′	σ
30	13.4	21.4	18.5	3.6	1.8	3.8	23.3	35.0	23.0	38.1
34	12.0	23.2	17.2	3.5	2.0	3.7	21.0	38.4	20.6	41.3
38	10.8	24.7	15.9	3.5	2.1	3.6	19.1	41.3	18.7	44.0
42	9.9	25.9	14.9	3.4	2.3	3.5	17.6	43.9	17.1	46.4
46	9.1	26.9	13.9	3.3	2.4	3.4	16.2	46.2	15.7	48.5
50	8.5	27.7	13.1	3.3	2.5	3.4	15.1	48.2	14.6	50.3
54	8.0	28.4	12.3	3.2	2.6	3.3	14.1	50.0	13.7	51.9
58	7.5	28.9	11.7	3.2	2.7	3.3	13.3	51.6	12.8	53.3
62	7.1	29.4	11.1	3.1	2.8	3.2	12.6	53.0	12.1	54.6
66	6.8	29.8	10.6	3.1	2.9	3.2	11.9	54.3	11.5	55.8
70	6.6	30.2	10.1	3.1	3.0	3.2	11.4	55.5	11.0	56.8

Table 1

Electrical properties of tissues at different frequencies.

B. Quasi-static approximation

For estimation of the maximal values of the E-field in narrow blood vessels we applied the quasi-static theory. In order for the quasi-static theory to be applicable, the wavelength λ of the electromagnetic wave used for exposure should be much greater than the object size [Lin et al., 1973; Olver, 1992]. For example, λ of 42 GHz electromagnetic field in the skin and fat is equal to 2.0 and 3.8 mm, respectively. The sizes of the fat layer and blood vessels were ≤ 0.2 mm, and being significantly smaller than λ satisfied the assumptions of the quasi-static theory.

As the normal components of the electric flux densities in the fat (D_{fat}) and skin (D_{skin}) are equal across a boundary of the two materials, the E-field in the fat layer (E_{fat}) can be found from the following equation:

$$Efat=|\varepsilon skin||\varepsilon fat|\cdot Eskin$$

(2)

In accordance with the quasi-static theory, E_{fat} would remain the same value throughout the whole fat layer. Hence, the E-field in the fat normalized to the E-field in skin (E_{skin}) is equal to the ratio of the absolute values of permittivities (PR) of skin and fat; that is, $PR=|\varepsilon_{skin}| / |\varepsilon_{fat}|$. The E-field in a blood vessel could reach its maximal value equal to the E_{fat} under the condition that the diameter of the vessel was extremely small and its length was great enough to minimize the outside edge effects [Feynman et al., 1964]. This follows the requirement that at a boundary between two dielectric media (fat and blood) the tangential components of the E-fields are continuous across the boundary. It was shown that the length of the blood vessel should be at least ten times greater than its diameter to satisfy these conditions [Alekseev and Ziskin, 2009a]. Otherwise, the E-field in the vessel would be lower, but proportional to the E-field in the fat.

RESULTS

A. Model I

Figure 3 shows that a blood vessel traversing the fat layer could absorb a significant amount of MMW energy depending on the orientation of the E-field. The maximal absorption occurred at the orientation of the E-field component parallel to the cylindrical axis of the blood vessel (Fig. 3(b)). The maximal SAR (SAR_{max}) in a blood vessel decreased quickly to its minimal value (SAR_{min}) while increasing the angle (β) between the cylindrical axis of the blood vessel and the E-field. The dependence of the SAR on β was well fitted to the following equation:

$$SAR(\beta)=(SARmax-SARmin)\cos 2(\beta)+SARmin$$

(3)

The SAR distribution inside the blood vessel was not uniform. The SAR reached its maximal value in the region closest to the center of a blood vessel at the muscle layer side and dropped at the outside edges at both skin and muscle layer sides. The distortion of the SAR distribution outside the blood vessel was highly localized to the regions immediately surrounding the blood vessel (Fig. 3(a)).

The SAR in the blood vessel increased with decreasing diameter (Fig. 4, curve 1). The dependence of the SAR on the diameter (d) of a blood vessel was well described by the following exponential function:

$$nSAR=Aoe-ddo+1$$

(4)

where A_o and d_o are constants. A_o was not dependent on a length of a blood vessel l and was equal to 31.4, while d_o increased with increasing l. At l = 0.2 mm d_o =0.09. As can be seen from Fig. 4, curve 1, and Eq. 4, the maximal nSAR in very small blood vessels such as capillaries may reach 32.4. The quasi-static estimation of the maximal SAR gives a value of 32.5, which is very close to that found from the FDTD calculations.

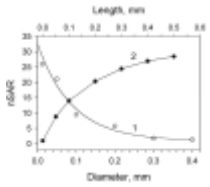

Figure 4

Dependence of the normalized SAR on the size of a blood vessel. (1) The normalized SAR versus the diameter of the blood vessel. Solid line is a fit to Eq. 4. (2) The normalized SAR versus the length of the blood vessel. Diameter of the blood vessel is **...**

The SAR in a blood vessel was sensitive to changes in the skin and fat thicknesses. Unlike human tissue, the murine skin has smaller variations in tissue thicknesses [Anderson et al., 2010]. In our calculations we used typical variations in thicknesses of different tissues of murine skin. At a given diameter of a blood vessel, the SAR in a blood vessel increased with increasing the thickness of the fat layer or length of the blood vessel (Fig 4, curve 2). Variation in the skin thickness by 20% produced much lower changes (≤ 3%) of the SAR in a blood vessel.

Figure 5 shows the E-field amplitude distributions in blood vessels of different diameters and in the surrounding tissues. The E-field in a blood vessel increased significantly with decreasing the blood vessel diameter, reaching the E-field in the fat layer. The maximal value of the normalized E-field in the fat layer was equal to 4.27. A similar result (nE_{fat} = 4.26) was obtained from Eq. 2 of the quasi-static approximation. The larger blood vessels produced greater disturbances of the E-field distributions in the fat, skin and muscle layers.

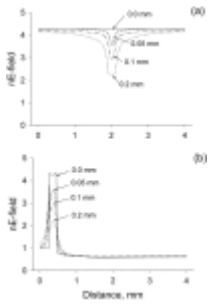

Figure 5

E-field distributions in blood vessels of different diameters and surrounding tissue. (a) E-field profiles drawn through the center of a blood vessel parallel to the H-field (Fig. 1). (b) E-field profiles drawn through the center of a blood vessel parallel **...**

The E-field amplitude in a blood vessel slowly declined with increasing the frequency from 30 to 80 GHz (Fig. 6). The calculated data points were well fitted to the ratio of the absolute values of permittivity of skin, and fat multiplied by a factor of 0.75. These results were obtained for a blood vessel with the diameter of 0.05 mm. With decreasing the diameter of a blood vessel this factor tended to reach 1.0. In this case, the E-field in a blood vessel approached the E-field in the fat layer, found from Eq. 2 (Fig. 6, curve 1).

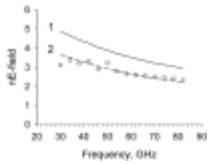

Figure 6

Frequency dependence of the normalized E-field amplitude in a blood vessel traversing a 0.2 mm fat layer. The diameter of the blood vessel is 0.05 mm. Curves (1) and (2) represent the ratio of the absolute values of permittivity of skin and fat, PR, and **...**

The SAR in paired blood vessels in close contact with each other was lower than that in a single blood vessel under the same exposure conditions (Fig. 7). In blood vessels with a diameter of 0.05 mm, the SAR was reduced by 13%. At larger diameters the SAR drop was greater. However, with increasing distance between blood vessels the SAR slowly regained its original value in a single blood vessel.

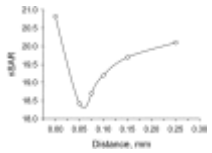

Figure 7

Dependence of the peak normalized SAR in paired blood vessels on the distance between their centers. Diameter of the blood vessel is 0.05 mm.

Model II

When the cylindrical model of murine limb was exposed to plane MMW, the absorption of MMW energy by the skin and blood vessels located around the limb was not uniform (Fig. 8). The maximal and minimal absorption of incident energy by skin occurred on the front and rear surfaces of the limb, respectively. However, the SAR maximums and minimums were not located at 0° and ±180° but at ±15 and ±150°, respectively (Fig. 8 (b)). The distribution of the SAR in blood vessels was different from that in the skin. More MMW energy was absorbed by the blood vessels located on the flank areas of the limb at ±75 and ±145°. At these areas the maximal SAR values were comparable to or greater than the maximal SAR in the skin. In blood vessels located on the front and rear areas of the limb the SAR was minimal.

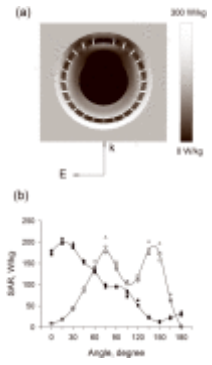

Figure 8

SAR distribution in the cylindrical model of a murine limb. (a) Cross-sectional view. The external diameter of a limb is 4 mm. The diameter of a bone is 2 mm. (b) SAR in the skin and blood vessels versus the radial angle of their location for different **...**

Inclusion of bone in the cylindrical model did not produce notable modification of the SAR distributions in the skin and blood vessels (Fig. 8(b)). The SAR distributions in the limb with bone diameters of 1.5–2.0 mm did not differ from the SAR distributions in the limb in the absence of bone (control). At the greater bone diameter, there was a slight enhancement of the MMW absorption by blood vessels. We can explain this by the fact that the influence of the bone on the MMW interaction with the limb increases as the distance between the bone and skin surface becomes closer to the penetration depth of MMW (0.85–0.93 mm at 42.25 GHz) [Alekseev et al., 2008b].

The diameter of the limb played a great role in MMW absorption. With decreasing the diameter of the limb the maximal SAR in the skin reduced. At the same time, the maximal SAR in blood vessels located at ±135° increased significantly (Fig. 9 (a)). In the limb with the diameter of 3 mm the SAR in the blood vessels located at ±135° was 2.4 times greater than the maximal SAR in the skin. Figure 9 (b) illustrates the distribution of the SAR in blood vessels normalized to the SAR in the skin located next to each blood vessel. The maximal nSAR in the 3 mm limb was equal to 14. This value was lower than the maximal SAR, equal to 20.8, obtained from model I at the orientation of the blood vessel parallel to the E-field. Because the incident plane wave had the E-field component directed along its front, the blood vessels located at the front surface of the limb had a perpendicular orientation to the E-field and absorbed minimal energy. It seemed that due to the complex interaction of a plane wave with a cylindrical limb, the front of a plane wave changed its direction in the flank areas of the limb. Analysis of the propagation of the electromagnetic wave confirmed this suggestion. At ±135° the E-field was close to but did not achieve a perfectly parallel orientation to a blood vessel.

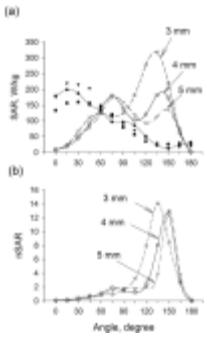

Figure 9

Absolute value of the SAR (a) and nSAR (b) versus the radial angle at different diameters of the cylindrical model of a murine limb: 3 mm (squares), 4 mm (circles), and 5 mm (triangles). The bone diameter is 0 mm. Open and filled symbols in (a) stand **...**

In the elliptical models of the limb the SAR distributions in the blood vessels were similar to those obtained for the cylindrical model (Fig. 10). The SAR in the skin was maximal in the front surface of the limb and minimal in the rear surface. At both orientations of the model, as shown in Figure 10, the maximal absorption of MMW energy by blood vessels occurred at the lateral faces of the elliptical models at ±135–145°. However, at the parallel orientation of

the E-field to the major axis of the ellipse, the SAR values in the blood vessels at the same locations were greater.

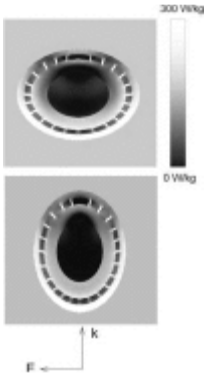

Figure 10

Cross-sectional view of the SAR distributions in the elliptical model of a murine limb at the parallel and perpendicular orientations of the major axis of the ellipse to the E-field. The major and minor axes of the external ellipse are 4 and 3 mm, respectively. **...**

Go to:

DISCUSSION

In our recent study we showed that cutaneous blood vessels could absorb MMW energy by ~40% greater than the surrounding dermis [Alekseev and Ziskin, 2009a]. Quantitatively similar absorption of MMW energy was obtained for the blood vessels located in the fat layer and oriented parallel to the skin surface and the E-field. The enhanced absorption of MMW energy by blood vessels was due to the greater conductivity of the blood than that of the surrounding tissue. The maximal internal E-field in the long narrow blood vessel was achieved at the parallel orientation of the blood vessel to the external E-field. In this case it was equal to the E-field in the surrounding tissue.

In the present calculations we found that the maximal SAR in blood vessels normally traversing the fat layer could be more than 30 times greater than that in the skin. In this case the SAR increased not only due to the higher blood conductivity but also to the enhanced amplitude of the E-field within the blood vessel. The SAR increased with decreasing the blood vessel diameter and increasing the fat thickness. These results could be well understood on the basis of the quasi-static theory. According to the quasi-static approach the E-field throughout the fat layer could be determined using Eq. 2. Due to the low permittivity of fat, the E-field in the fat layer is greater than in the skin and muscle layers. Though the conductivity of fat is much lower than that of skin and muscle, the greater value of the SAR in the fat layer (Fig. 3) was due to the higher amplitude of the E-field in the fat layer. With decreasing the diameter of the blood vessel and increasing its length, i.e., the thickness of the fat layer, the E-field in a blood vessel tends to achieve its maximal value, given by Eq. 2. In paired vessels located very close to each other the effective size of the vessels is greater than the diameter of each single vessel. Therefore, the E-field and consequently the SAR are reduced. With increasing the distance between the vessels the E-field slowly regained its original value for a single vessel, i.e., the vessels at longer distances can be considered as isolated single vessels.

The SAR in a blood vessel was very critical to changes of the angle β between the blood vessel axis and the E-field (Eq. 3). This can be explained by the fact that the E-field in a blood vessel is proportional to cos(β). The absorption remained close to the maximal value only at angles less than ±15°.

Figure 6 demonstrates that the SAR in a blood vessel smoothly increased by 43% with decreasing the frequency from 61.22 to 42.25 GHz, revealing no resonance-type absorption at the therapeutic frequencies. This means that the absorption of MMW by blood vessels does not play a great role in the frequency dependence of the therapeutic effects.

At the normal incidence of the mm plane wave on a relatively flat skin surface, the E-field component lies parallel to the fat layer and is perpendicular to the axis of blood vessels traversing the fat layer. In this case the SAR in blood vessels would be minimal. However, when exposing the small parts of the animal body such as limbs, fingers and tails, the angle between the E-field and the skin is changed and may become nearly perpendicular to the fat layer. In this case the SAR in blood vessels increases significantly and can be even greater than that in the skin on the front surface.

The perpendicular orientation of the E-field to the skin surface can be directly realized when the skin is exposed with a waveguide operating in the TM modes. We know, for example, that in the TM_{11} mode the E-field is directed along the k-vector, i.e., in the direction of traveling of the electromagnetic field. Exposing a relatively flat skin surface with an open-ended waveguide operating in the TM_{11} mode, the E-field would be automatically directed perpendicular to the skin surface.

We have previously reported the results of calculations of the SAR distribution in murine skin exposed to MMW with the IPD of 10 mW/cm^2 [Alekseev et al., 2008b]. We found that the SAR in the dermis near the boundary with the fat layer was about 100 W/kg. For the therapeutic intensities of 10–30 mW/cm^2 the SAR would be in the range of 100–300 W/kg. The maximal SAR in blood vessels with the diameter of 50 μm traversing the fat layer is about 20 times greater than in the skin. This gives the absolute values of the SAR in blood vessels equal to 2000–6000 W/kg. In small blood vessels like capillaries these values would be even greater. The significant absorption of MMW energy by blood vessels may produce overheating of the blood. However, to determine the actual temperature elevation it is necessary to perform accurate calculations of the temperature rise using the heat transfer equations and taking into the account that the blood flow in the vessels would significantly reduce the steady-state temperature rise.

Because the blood vessels are innervated by autonomic nerves [Bloom and Fawcett, 1968], it is very important to estimate the E-field in the walls of blood vessels. Though our models did not include the blood vessel walls due to lack of dielectric data we can make some estimations of the E-field distributions in the walls. In the narrow blood vessels the E-field in blood and walls would be very close to that in the fat layer. With increasing the diameter of the blood vessel, the E-field in the center of the blood vessel decreases (Fig. 5). However, in the wall contacting the fat the E-field will be close to that in the fat layer.

Thus, MMW exposure of murine skin can produce significant absorption of MMW energy in blood vessels traversing the fat layer. Stimulations of autonomic nerve endings innervating blood vessels and some receptors on the endothelium evoke nitric oxide release [Joyner and Dietz, 1997]. The latter contributes to the regulation of hyperemic responses in skin.

Enhanced values of the SAR and E-field in the blood vessels may play a primary role in initiating MMW effects on blood cells and nitric oxide release resulting in vasodilatation of blood vessels. The obtained results are important for MMW dosimetry of murine skin and for understanding the possible mechanisms of the biological effects of MMW.

Acknowledgments

Grant sponsor: NIH NCCAM, Grant number P01-AT002025.

Go to:

REFERENCES

1. Algire GH. Determination of peripheral blood pressure in unanesthetized mice during microscopic observation of blood vessels. J Natl Cancer Inst. 1954;14:865–877. [PubMed]
2. Alekseev SI, Ziskin MC. Distortion of millimeter-wave absorption in biological media due to presence of thermocouple and other objects. IEEE Trans Biomed Eng. 2001;48:1013–1019. [PubMed]
3. Alekseev SI, Radzievsky AA, Logani MK, Ziskin MC. Millimeter wave dosimetry of human skin. Bioelectromagnetics. 2008a;29:65–70. [PubMed]
4. Alekseev SI, Gordiienko OV, Ziskin MC. Reflection and penetration depth of millimeter waves in murine skin. Bioelectromagnetics. 2008b;29:340–344. [PubMed]
5. Alekseev SI, Ziskin MC. Millimeter-wave absorption by cutaneous blood vessels: A computational study. IEEE Trans Biomed Eng. 2009a;56:2380–2388. [PubMed]
6. Alekseev SI, Ziskin MC, Fesenko EE. On mechanism of action of microwaves on bilayer lipid membranes: Role of a membrane-forming hole in the Teflon film. Biofizika. 2009b;54:488–491. [PubMed]
7. Alekseev SI, Fesenko EE, Ziskin MC. Enhanced absorption of microwaves within cylindrical holes in Teflon film. IEEE Trans Biomed Eng. 2010;57:2517–2524. [PubMed]
8. Anderson V, Croft R, McIntosh RL. SAR versus S_{inc}: What is the appropriate RF exposure metric in the range 1–10 GHz? Part I: Using planar body models. Bioelectromagnetics. 2010;31:454–466. [PubMed]
9. Bloom W, Fawcett DW. A Textbook of Histology. 9th edition Saunders; Philadelphia: 1968. pp. 479–509.
10. Braverman IM. Ultrastructure and organization of the cutaneous microvasculature in normal and pathologic states. J Invest Dermatol. 1989;93:2S–9S. [PubMed]
11. Dang Y-Y, Ren Q-S, Liu H-X, Zhang J-S. Comparison of histologic, biochemical, and mechanical properties of murine skin treated with the 1064-nm and 1320-nm Nd: YAG lasers. Exp Dermatol. 2005;14:876–882. [PubMed]
12. Duck FA. Physical properties of tissue: A comprehensive reference book. Academic Press; San Diego, CA: 1990. pp. 137–143.
13. Eibert TF, Alaydrus M, Wilczewski F, Hansen VW. Electromagnetic and thermal analysis for lipid bilayer membranes exposed to RF fields. IEEE Trans Biomed Eng. 1999;46:1013–1021. [PubMed]
14. Feynman RP, Leighton RB, Sands M. The Feynman Lectures on Physics. Vol 2. Addison-Wesley Publishing; Reading, MA: 1964. Chapter 11; pp. 1–11.
15. Gabriel S, Lau RW, Gabriel C. The dielectric properties of biological tissues: III. Parametric models for the dielectric spectrum of tissues. Phys Med Biol. 1996;41:2271–2293. [PubMed]

16. Gapeev AB, Safronova VG, Chemeris NK, Fesenko EE. Modification of the activity of murine peritoneal neutrophils upon exposure to millimeter waves at close and far distances from the emitter. Biofizika. 1996;41:205–219. [PubMed]
17. Gapeyev AB, Mikhalik EN, Chemeris NK. Anti-inflammatory effects of low-intensity high-frequency electromagnetic radiation: Frequency and power dependence. Bioelectromagnetics. 2008;29:197–206. [PubMed]
18. Grover J, Lee ER, Mounkes LC, Stewart CL, Roughley PJ. The consequence of PRELP overexpression on skin. Matrix Biol. 2007;26:140–143. [PubMed]
19. Jauchem JR, Ryan KL, Frei MR. Cardiovascular and thermal responses in rats during 94 GHz irradiation. Bioelectromagnetics. 1999;20:264–267. [PubMed]
20. Jauchem JR, Ryan KL, Tehrany MR. Effects of histamine receptor blockade on cardiovascular changes induced by 35 GHz radio frequency radiation heating. Auton Autocoid Pharmacol. 2004;24:17–28. [PubMed]
21. Joyner MJ, Dietz NM. Nitric oxide and vasodilation in human skin. J Appl Physiol. 1997;83:1785–1796. [PubMed]
22. Kunz KS, Luebbers RJ. The Finite Difference Time Domain Method for Electromagnetics. CRC Press; Boca Raton, FL: 1993. p. 448.
23. Lin JC, Guy AW, Johnson CC. Power deposition in a spherical model of man exposed to 1–20 MHz electromagnetic fields. IEEE Trans Microwave Theory Tech MTT. 1973;21:791–797.
24. Maloney JG, Kesler MP. Taflove A (editor): Advances in Computational Electrodynamics: The Finite-Difference Time-Domain Method. Artech House; Norwood, MA: 1998. Analysis of periodic structures; pp. 345–407.
25. Olver AD. Microwave and Optical Transmission. John Wiley and Sons; New York: 1992. pp. 71–89.
26. Rojavin MA, Ziskin MC. Medical application of millimeter waves. Q J Med. 1998;91:57–66. [PubMed]
27. Radzievsky AA, Rojavin MA, Cowan A, Alekseev SI, Ziskin MC. Hypoalgesic effect of millimeter waves in mice: Dependence on the site of exposure. Life Sci. 2000;66(21):2101–2111. [PubMed]
28. Radzievsky AA, Gordiienko OV, Alekseev SI, Szabo I, Cowan A, Ziskin MC. Electromagnetic millimeter wave induced hypoalgesia: Frequency dependence and involvement of endogenous opioids. Bioelectromagnetics. 2008;29:284–295. [PubMed]
29. Roshchupkin DI, Kramarenko GG, Anosov AK. Effect of extremely high frequency electromagnetic radiation and ultraviolet radiation on aggregation of thymocytes and erythrocytes. Biofizika. 1996;41:866–869. [PubMed]
30. Zweifach BW, Kossman CE. Micromanipulation of small blood vessels in the mouse. Am J Physiol. 1937;120:23–35.